Variational Quantum Shot-Based Simulations for Waveguide Modes

Emanuel Colella, Spencer Beloin, Luca Bastianelli, *Member, IEEE*, Valter Mariani Primiani, *Senior Member, IEEE*, Franco Moglie, *Senior Member, IEEE*, and Gabriele Gradoni, *Member, IEEE*

***Abstract*— Current quantum computers (QCs) belong to the noisy intermediate-scale quantum (NISQ) class, characterized by noisy qubits, limited qubit capabilities, and limited circuit depth. These limitations have led to the development of hybrid quantum-classical algorithms that split the computational cost between classical and quantum hardware. Among the hybrid algorithms, the variational quantum eigensolver (VQE) is mentioned. The VQE is a variational quantum algorithm designed to estimate the eigenvalues and eigenvectors of a system on universal-gate quantum architectures. A canonical problem in electromagnetics is the computation of eigenmodes within waveguides. Following the finite difference method, the wave equation can be recast as an eigenvalue problem. This work exploits the quantum superposition and entanglement in quantum computing to solve the square waveguide mode problem. This algorithm is expected to demonstrate exponentially efficiency over classical computational techniques as the qubit count increases. The simulations were performed on IBM's three-qubit quantum simulator, Qasm IBM Simulator. A shot-based simulation was performed considering computationally based measurements of the quantum hardware. The results of the probabilistic readout, reported in terms of 2-D eigenmode field distributions, are close to ideal values with a few number of qubits, confirming the possibility to exploit the quantum advantage to formulate innovative eigensolvers.**

***Index Terms*— Hamiltonian simulation, Helmholtz equation, quantum computing, variational quantum eigensolver (VQE), waveguide modes.**

I. Introduction

A QUANTUM computer (QC) is a calculator that exploits quantum principles such as superposition, entanglement, and tun neling to perform operations on data [1], [2]. QCs were proposed by Richard Feynman in 1981 specifically for modeling quantum systems, whose complexity is too great to be adequately described using classical computation [3]. Since their introduction, QCs have undergone several decades of theoretical development in tandem with a significant increase in experimental capability to realize qubits and implement quantum circuits [4]. QCs have the goal of offering time complexity and energy efficiency advantages over classical computers [5]. Achieving practical quantum advantage in quantum simulations has proved possible [6] but it comes at the cost of solving experimental challenges. Among these, it is important to consider the issue of quantum decoherence and noise in quantum computing architectures, for which quantum error corrections methodologies have been developed and improved over the years.

The scientific community has been seeking to identify problems where quantum computation solutions possess the greatest advantage [7], [8]. Currently there are several large technology companies working on quantum computing, including superconducting (IBM, Google, Rigetti Computing), trapped ion qubit (IonQ, Honeywell), quantum annealing (D-Wave), spin qubits (Intel), cold atoms (Atom Computing), etc., [9], [10].

We are currently in the era of noisy intermediate-scale quantum (NISQ) machines [11], [12]. This era is defined by the current limitations of quantum hardware such as quantum circuit depth, number of qubits, and noise, which results in a significant reduction of accuracy with the number of operations completed [13]. Due to these limitations, hybrid classical-quantum computing–a strategy that uses joint classical computation and existing quantum hardware–must be used to solve prescribed algorithms [14]. This class of algorithms is known as VQA [15]. The VQA belongs to set of hybrid classical-quantum algorithms for quantum simulations that minimize cost functions to find the ground state and the excited states of a physical system using variational quantum circuits [12], [16].

According to the Bharadwaj-Sreenivasan classification [17], reproduced here in Fig. 1, eigenvalue solvers constitute an important part of quantum algorithms adopted in many branches of engineering.

This current work discusses application of the variational quantum eigensolver (VQE) to solve the waveguide mode problem described by the Helmholtz equation. It is an extension of the work in [18]. Thus far, problems in the fields

Manuscript received 31 August 2023; revised 23 November 2023; accepted 26 November 2023. Date of publication 19 December 2023; date of current version 4 April 2024. This work was supported in part by the Royal Society Industry Fellowship under Grant INF\R2\192066 and in part by EPSRC under Grant EP/V048937/1 and Grant EP/X038491/1. *(Corresponding author: Emanuel Colella.)*

Emanuel Colella, Luca Bastianelli, Valter Mariani Primiani, and Franco Moglie are with the Dipartimento di Ingegneria dell'Informazione, Università Politecnica delle Marche, 60131 Ancona, Italy, and also with the Consorzio Nazionale Interuniversitario per le Telecomunicazioni (CNIT), 43124 Parma, Italy (e-mail: e.colella@pm.univpm.it; l.bastianelli@pm.univpm.it; v.mariani@univpm.it; f.moglie@univpm.it).

Spencer Beloin is with the HPM Effects and Modeling and Simulations Group, Naval Surface Warfare Center Dahlgren Division, Dahlgren, VA 22448 USA (e-mail: spencer.t.beloin.civ@us.navy.mil).

Gabriele Gradoni is with the Department of Electrical and Electronic Engineering, University of Surrey, GU2 7XH Guildford, U.K., and also with the Department of Computer Science and Technology, University of Cambridge, CB2 1TN Cambridge, U.K. (e-mail: g.gradoni@surrey.ac.uk).

Color versions of one or more figures in this article are available at https://doi.org/10.1109/TMTT.2023.3339243.

Digital Object Identifier 10.1109/TMTT.2023.3339243

of chemistry and fluid dynamics, as well as thermodynamics and power electronics, have exploited the use of quantum algorithms. The same trend is developing in electromagnetic engineering, where quantum computing has been used to design antenna arrays [19] and metasurfaces [20]. The accurate computation of electric and magnetic eigenmodes of waveguides with arbitrary cross sections [21] is a challenging task that requires sophisticated numerical methods to improve the associated computational complexity [22]. These modes are determined by the geometry, dimensions, and material composition of the waveguide. An advantage is theoretically obtainable by mapping the canonical numerical solution of the wave equation onto a simple numerical scheme that can be implemented on next-generation quantum computing architectures [23]. For example, using the finite difference method, the Helmholtz equation modeling transverse electric (TE) and transverse magnetic (TM) eigenmodes can be discretized and broken up into algebraic equations which can be expressed as a system of linear equations [24].

The seminal paper Harrow et al. [25] demonstrated that solving sparse systems of linear equations represented by matrices with small condition numbers by the HHL algorithm can be accomplished exponentially faster on quantum devices than their classical counterparts [26]. Unfortunately, current and near term future hardware is incapable of supplying enough qubits to fully execute this algorithm. To account for this current deficiency, Ewe et al. [15] have proposed using the VQE algorithm to model TE and TM wave propagation on current and near term computational hardware. VQE is a type of VQA that minimizes a given cost function to find the eigenvalues and eigenmodes of a physical system described by an eigenvalue equation. To achieve this, the Authors utilize the Hamiltonian decomposition proposed in [27], which expresses the Hamiltonian of the system as a linear combination of unitary operators, namely I, the identity matrix, X, the X-Pauli rotation operator, and P_n, the cyclic shift operator implemented using the multi-control Toffoli gate [28], [29], [30]. By leveraging this mathematical formulation, the Authors demonstrate that VQE offers an effective solution for solving the Helmholtz's equation for waveguide modes. Herein, we adopt the formulation of VQE proposed by Peruzzo et al. [31], employing the canonical Pauli decomposition of the Hamiltonian, with a change of basis to simulate measurements in computational basis, thus mimicking the actual readout procedure on real quantum hardware. Therefore, the objective of the paper is to exploit the quantum principles of superposition and entanglement in quantum computing to solve the waveguide mode problem. In particular, it allows us to solve exponentially numerical domains as the qubit count increases. This is performed by a shot [28] based-quantum simulation in computational basis that emulate the behavior and hardware limitations of real QCs [28].

Specifically, our focus lies on a three-qubit simulation of waveguide modes by VQE algorithm. This approach allows us to replicate the probabilistic nature of current NISQ computers, making it feasible for implementation on existing quantum hardware.

II. Quantum Formulation

A. Waveguide Modes

Waveguide modes are distributions of transverse and longitudinal components of electric and magnetic fields within structures that confine electromagnetic waves along guided paths [21]. Two different types of waves can propagate inside such structures, TE and TM waves. For TM waves, the magnetic field is perpendicular to the direction of propagation, while the electric field is parallel. In the case of TE waves, the electric field is perpendicular to the direction of propagation, while the magnetic field is parallel. Let us analyze a cross section of a rectangular hallow metallic waveguide shown in Fig. 2. It is assumed that the waveguide is a square filled with a material with specific electrical permittivity ε and magnetic permeability μ. The choice of a square lies above its degenerate modes being the most challenging in electromagnetics. The distribution of the electromagnetic fields within a waveguide is described by the Helmholtz equation, for TE and TM cases

$$-\frac{\partial^2 E_z}{\partial x^2}-\frac{\partial^2 E_z}{\partial y^2}=k_s^2 E_z, \quad \text{for TM modes} \tag{1}$$

$$-\frac{\partial^2 H_z}{\partial x^2}-\frac{\partial^2 H_z}{\partial y^2}=k_s^2 H_z, \quad \text{for TE modes} \tag{2}$$

where $k_s^2=k^2-k_z^2$, $k=(\omega^2\mu\varepsilon)^{1/2}$ is the wavenumber inside the waveguide, ω the angular frequency, and k_z the propagation constant along z-direction. To solve the Helmholtz equation for rectangular waveguide, the boundary conditions for the electric and magnetic fields are considered. In case of TE waves, the magnetic component H_z must satisfy the Neumann boundary condition

$$\frac{\partial H_z}{\partial x}(0,y)=\frac{\partial H_z}{\partial x}(a,y)=\frac{\partial H_z}{\partial y}(x,0)=\frac{\partial H_z}{\partial y}(x,b)=0. \tag{3}$$

For TM waves, the component of the electric field E_z must satisfy the Dirichlet boundary condition

$$E_z(0,y)=E_z(a,y)=E_z(x,0)=E_z(x,b)=0. \tag{4}$$

The two partial differential equations can be solved by separating the variables, i.e., by solving the equation for x and y separately, and then multiplying them together to get the two-variable solution of the Helmholtz equation. The separation of variables allows us to solve the following equation:

$$-\frac{d^2 f}{dl^2}=k_s^2 f \tag{5}$$

where $f\in\{E_z, H_z\}$ and $l\in\{x,y\}$, according to the modes. To solve the equations numerically, the central finite difference method has been adopted to approximate the second-order derivative as follows:

$$\frac{d^2 f}{dl^2}\approx\frac{f_{i+1}-2f_i+f_{i-1}}{\Delta l^2}. \tag{6}$$

Using this approximation, (5) can be written as a system of linear equations in matrix form of the type $Af=b$ whose dimension depends on the length of the vector f that you want

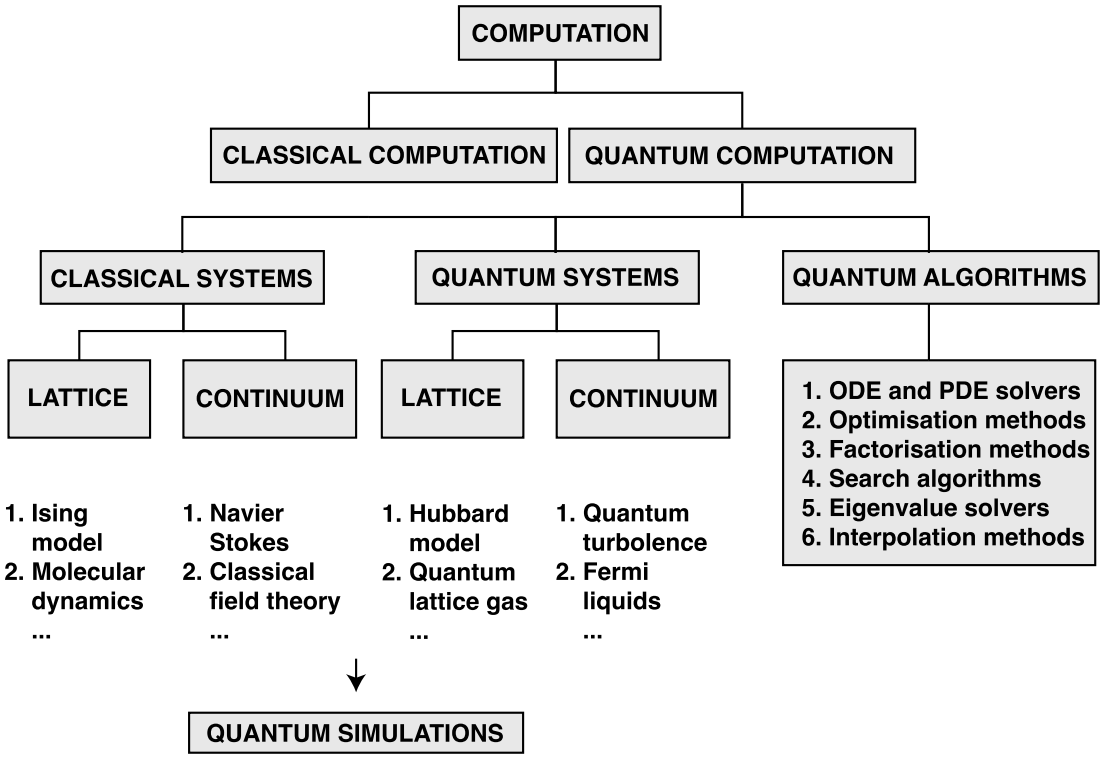

Fig. 1. Bharadwaj-Sreenivasan classification of quantum simulations.

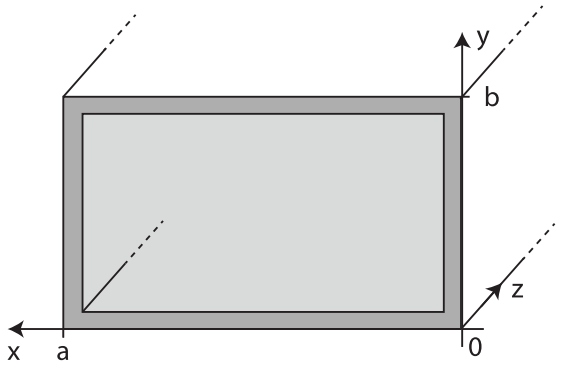

Fig. 2. Rectangular waveguide of width a along x and height b along y.

to obtain [32]. Furthermore, being a homogeneous equation, it may be represented as an eigenvalue equation as follows:

$$Af = k_s^2 f \tag{7}$$

where A is the matrix of the coefficients of Helmholtz equation in matrix form while $f \in \{E_z, H_z\}$ [22], [32].

B. Hamiltonian Simulation

Writing (1) and (2) in matrix form (7), the Helmholtz equation represented as an eigenvalue equation can be solved by finding the eigenvalues k_s^2 and eigenvectors f, also called eigenmodes, of matrix A. The eigenvalues define the mode excitation frequencies [33] while the eigenvectors identify E_z or H_z in the cross section of the waveguide. In quantum mechanics, the eigenvalue problem can be solved using the variational method to find approximations of the lowest energy state, called the ground state, and some excited states of complex quantum systems. Using the Dirac notation, (7) can be expressed as follows:

$$\mathcal{H}|\psi\rangle = E|\psi\rangle \tag{8}$$

where $\mathcal{H}$ is the Hamiltonian operator associated with the matrix A, $|\psi\rangle$ is the quantum state, also called eigenstate, associated with the eigenvector f in Hilbert space and E the energy level associated with the eigenvalue k_s^2 in the quantum system. Considering a three-particle quantum system (see three qubit simulation, described in Section II-C), the dimension of $|\psi\rangle$ is 2^3, thanks to quantum superposition. Therefore, the size of $\mathcal{H}$ is $2^3 \times 2^3$ for (8). Considering the TM case, the Hamiltonian operator becomes [15]

$$\mathcal{H}_{\text{TM}} = \frac{1}{\Delta l^2}\begin{pmatrix} 3 & -1 & 0 & 0 & 0 & 0 & 0 & 0 \\ -1 & 2 & -1 & 0 & 0 & 0 & 0 & 0 \\ 0 & -1 & 2 & -1 & 0 & 0 & 0 & 0 \\ 0 & 0 & -1 & 2 & -1 & 0 & 0 & 0 \\ 0 & 0 & 0 & -1 & 2 & -1 & 0 & 0 \\ 0 & 0 & 0 & 0 & -1 & 2 & -1 & 0 \\ 0 & 0 & 0 & 0 & 0 & -1 & 2 & -1 \\ 0 & 0 & 0 & 0 & 0 & 0 & -1 & 3 \end{pmatrix} \tag{9}$$

where the first and last rows refer the Dirichlet boundary conditions ([15], see Appendix). For TE modes, the Hamiltonian

operator becomes [15]

$$\mathcal{H}_{\mathrm{TE}} = \frac{1}{\Delta l^2}\begin{pmatrix} 1 & -1 & 0 & 0 & 0 & 0 & 0 & 0 \\ -1 & 2 & -1 & 0 & 0 & 0 & 0 & 0 \\ 0 & -1 & 2 & -1 & 0 & 0 & 0 & 0 \\ 0 & 0 & -1 & 2 & -1 & 0 & 0 & 0 \\ 0 & 0 & 0 & -1 & 2 & -1 & 0 & 0 \\ 0 & 0 & 0 & 0 & -1 & 2 & -1 & 0 \\ 0 & 0 & 0 & 0 & 0 & -1 & 2 & -1 \\ 0 & 0 & 0 & 0 & 0 & 0 & -1 & 1 \end{pmatrix} \tag{10}$$

where the first and last rows are determined by Neumann boundary conditions ([15], see Appendix). Let us decompose the Hamiltonian operators by Pauli decomposition allowing us to write the Hamiltonian operators as a linear combination of Pauli matrices I, X, Y, Z which form a basis for Hermitian matrices in dimensions that are powers of 2, as follows:

$$\mathcal{H} = \sum_i \alpha_i \mathcal{P}_i \tag{11}$$

with α_i the coefficients of the Pauli linear combination, $\mathcal{P}_i$ is the Pauli string with

$$X = \begin{pmatrix} 0 & 1 \\ 1 & 0 \end{pmatrix}, \quad Y = \begin{pmatrix} 0 & -i \\ i & 0 \end{pmatrix}, \quad Z = \begin{pmatrix} 1 & 0 \\ 0 & -1 \end{pmatrix}. \tag{12}$$

X, Y and Z are the Hermitian matrices which define the rotation of $|\psi\rangle$ around the x-, y-, and z-axis of the Bloch Sphere [28]. This decomposition is especially useful in quantum information and quantum computing, where Pauli operators play a crucial role in error correction, gate implementation, and quantum algorithms. Considering a unitary Δl, the $\mathcal{H}_{\mathrm{TM}}$ can be decomposed as follows [28]:

$$\begin{aligned} \mathcal{H}_{\mathrm{TM}} = {} & 2.25\ III - 1.0\ IIX - 0.5\ IXX - 0.5\ IYY \\ & + 0.25\ IZZ - 0.25\ XXX + 0.25\ XYY \\ & - 0.25\ YXY - 0.25\ YYX + 0.25\ ZIZ + 0.25\ ZZI \end{aligned} \tag{13}$$

while the matrix $\mathcal{H}_{\mathrm{TE}}$ [28]

$$\begin{aligned} \mathcal{H}_{\mathrm{TE}} = {} & 1.75\ III - 1.0\ IIX - 0.5\ IXX - 0.5\ IYY \\ & - 0.25\ IZZ - 0.25\ XXX + 0.25\ XYY - 0.25\ YXY \\ & - 0.25\ YYX - 0.25\ ZIZ - 0.25\ ZZI \end{aligned} \tag{14}$$

both referred to energy (J) where XXX is the Kronecker product of Pauli operators $X \otimes X \otimes X$, and the same for all the other Pauli strings.

C. Cost Function

The cost function to be minimized by VQE to find the ground state and the excited states of the system is defined as follows [31]:

$$c_m(\theta) = \langle\psi(\theta)|\mathcal{H}|\psi(\theta)|\rangle + \sum_{i=0}^{m-1} k_i \left|\langle\psi(\theta) \mid \psi\left(\theta^{(i)}\right)\rangle\right|^2 \tag{15}$$

where m is the mth excited state to be calculated, $|\psi(\theta)\rangle$ is the parameterized quantum state, that finds the solution of the Helmholtz equation. $\mathcal{H}$ is the Hamiltonian for the TM or TE systems, k_i a multiplicative constant such that $k_i > E_m - E_i$ while $\theta^{(i)}$ represents the set of parameters that minimize the cost function for the previous state [15], [31]. The cost function consists of two terms, the first term is the expectation value of the Hamiltonian operator while the second term forces the orthogonality between the quantum states $|\psi\rangle$, to be optimized and the previous found state $|\psi^i\rangle$. In particular, the expectation value represents the weighted average of all possible outcomes of a particular measurement on $|\psi\rangle$. In quantum mechanics, every measurable physical quantity is mathematically represented by an operator called an observable whose results of the measurements are the eigenvalues of the operator itself. In our case, the observable of our system is the Hamiltonian operator for the cases TM and TE. The Hamiltonian is the mathematical operator corresponding to the total energy of a system. Therefore, the results of the measurements of the Hamiltonian observable, i.e., its eigenvalues, are exactly the energy levels E into which the quantum system collapses upon measurement. Its spectrum is the set of all possible outcomes of the system's total energy. At the end of the measurement the quantum state collapses into a well-defined state represented by the eigenstate at specific energy level. To reduce the computational complexity, it is possible to calculate the expectation value of the Hamiltonian by evaluating the linear combination of expectation values of the simple Pauli contributions

$$\langle\mathcal{H}\rangle_\psi = \sum_i \alpha_i \langle\mathcal{P}_i\rangle_\psi \tag{16}$$

where $\langle\mathcal{P}_i\rangle_\psi$ denotes the expectation value of the $\mathcal{P}_i$ operator with respect to the state $|\psi\rangle$. In this way, the expectation value of each Pauli string, i.e., its eigenvalue, can be $\lambda = 1$ in the case the result of measurement is the classical bit 0 or $\lambda = -1$ in case that the result of measurement is the classical bit 1. The second term of the cost function is the forcing term which allows us to find that set of parameters forcing the orthogonalization of the states to be found. The term $\langle\psi(\theta)|\psi(\theta^i)\rangle$ represents the inner product between the state to be found $\langle\psi|$ and the previously found state $|\psi^i\rangle$. Overall, minimizing the cost function involves finding those sets of parameters θ that minimize the aforementioned inner product. Once we have found these eigenstates, and their corresponding eigenvalues, of the Hamiltonian we have solved the Helmholtz equation.

D. Pauli Basis Change

Current quantum hardware is not able to measure the x and y components of the quantum state vector but only the z component. This implies that for each Pauli string it is necessary to introduce a specific quantum measurement circuit which allows the quantum state vector to be rotated to get measurements along z-axis. This rotation allows the state vector to be rotated appropriately so as to measure the x and y components along z-axis. The Pauli string III is the identity matrix, therefore $\langle III\rangle_\psi = 1$, while ZZZ does not need a measuring quantum circuit since it is already in z basis. For all the remaining Pauli strings, a specific measuring quantum

circuit must be added to the ansatz. An ansatz is a parametric quantum circuit consisting of a sequence of quantum gates with tunable parameters applied to specific wires [16]. For the observable X, a Hadamard gate H needs to be added to the ansatz. The Hadamard gate rotates the state vector by π around the z-axis and by $\pi/2$ around the y-axis. For the observable Y, instead, it is necessary to add a conjugate transpose of phase gate $S^\dagger$ in series with a Hadamard gate. $S^\dagger$ gate rotates the state vector by $-\pi/2$ around the z-axis. Their matrix representation is shown below

$$H = \frac{1}{\sqrt{2}}\begin{pmatrix} 1 & 1 \\ 1 & -1 \end{pmatrix}, \quad S^\dagger = \begin{pmatrix} 1 & 0 \\ 0 & -i \end{pmatrix}. \tag{17}$$

For the observable I, on the other hand, it is necessary to add a CNOT gate which acts on two qubits: a control qubit and a target one. The control qubit is the qubit acted upon by the observable I while the target qubit is the first qubit of the system. The CNOT gate is defined as follows:

$$\text{CNOT} = \begin{pmatrix} 1 & 0 & 0 & 0 \\ 0 & 1 & 0 & 0 \\ 0 & 0 & 0 & 1 \\ 0 & 0 & 1 & 0 \end{pmatrix}. \tag{18}$$

The Pauli-based quantum measurement circuits for the Pauli observables of the three qubit Hamiltonian decomposition for TM and TE modes are reported in the Appendix.

III. VQE Implementation

The VQE relies on the variational method of quantum mechanics to find approximations to the ground state and excited states of a physical system. This method is based on the minimization of a cost function which allows for the calculation of the eigenvalues of the quantum system. In particular, the VQE is a hybrid classical-quantum algorithm that splits the computational task between classical and quantum hardware to overcome the current limitations of quantum machines. It exploits the computational power of the QC based on quantum superposition and quantum entanglement to evaluate the cost function and uses the classical computation to minimize the cost function. In our case the cost function is (15) whose minima represent the energy levels of the physical system while the eigenvectors represent its eigenstates. To define the cost function, the ansatz is needed. In the context of quantum computing, an ansatz, is a parameterized quantum circuit, that initializes a parameterized quantum state $|\psi(\theta)\rangle$. In our case, the hard efficient ansatz (HEA) has been initialized for both the TM and TE modes. HAE is a parameterized quantum circuit used in quantum computing to minimize the effect of noise and errors in quantum systems. The HEA is designed to be efficient in terms of computational resources, allowing for better management of complexity in quantum simulations. The HEA acts on an n-qubits register initialized to the computational basis state $|0^{\otimes n}\rangle$. This circuit consists of $R_y(\theta)$ and CNOT quantum gates. The $R_y(\theta)$ is the quantum gate that performs the rotation of the state vector around the y-axis of the Bloch sphere by an angle of θ acting on a single qubit. The CNOT gate, on the other hand, is the gate that performs quantum entanglement between two connected qubits. In the case of $n = 3$, the ansatz becomes

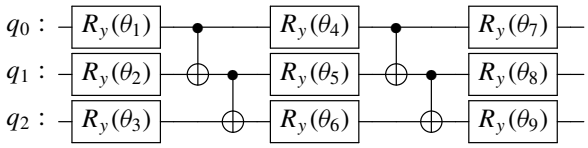

The state initialized by the ansatz is the following parameterized quantum state:

$$|\psi(\theta)\rangle = U(\theta)|0^{\otimes n}\rangle. \tag{19}$$

After the parameterized quantum circuit initialization, the starting set of parameters θ has been defined. The VQE algorithm starts by evaluating the cost function using the quantum hardware. The expectation value of the Hamiltonian is computed by evaluating the linear combination of the expectation values of simple Pauli terms, following the Hamiltonian decomposition defined in Section II. For each Pauli term there is an associated quantum measurement circuit, that joined to the ansatz allows us to measure the probability distribution of that Pauli string. From the probability distribution it is then possible to calculate the expectation value of that operator by calculating a weighted average of all possible outcomes for the observable. The result of the measurement of each Pauli string is a bitstring whose values denote the states that the qubits have collapsed into. Each bitstring is assigned a value which is given by the product of the eigenvalues $\lambda = 1$ or $\lambda = -1$ related to the classical states of the qubits 0 or 1, respectively. The forcing term is obtained by carrying out the absolute square of the inner product between the current state $|\psi(\theta)\rangle$ and the previously found one $|\psi(\theta)^i\rangle$. After evaluating the cost function using the set of initialized parameters, the result is passed to the classical hardware which updates the set of parameters to minimize the cost function by a classical optimization algorithm. A representative scheme of VQE is shown in Fig. 3. Upon investigation of several testing several minimization algorithms, Powell's Conjugate Gradient algorithm proved to be the most accurate. For this reason, Powell's Conjugate Gradient algorithm has been adopted. Powell's Conjugate Gradient method is classical minimization algorithm that permits calculation of the local minimum of a function. The advantage of this method lies in the fact that the cost function need not be differentiable, therefore its derivatives are not necessary. The method is based on a set of search vectors $\{s_1, \ldots, s_n\}$, each of which is aligned to each axis. The method minimizes the cost function through a bidirectional search of the local minimum along each search vector which can be performed using the Brent's method. Let the minima found after each iteration be

$$\left\{ x_0 + \alpha_1 s_1, x_0 + \sum_{i=1}^{2} \alpha_i s_i, \ldots, x_0 + \sum_{i=1}^{N} \alpha_i s_i \right\} \tag{20}$$

where x_0 is the initial search point while α_i is a coefficient obtained following each bidirectional search from vectors s_i.

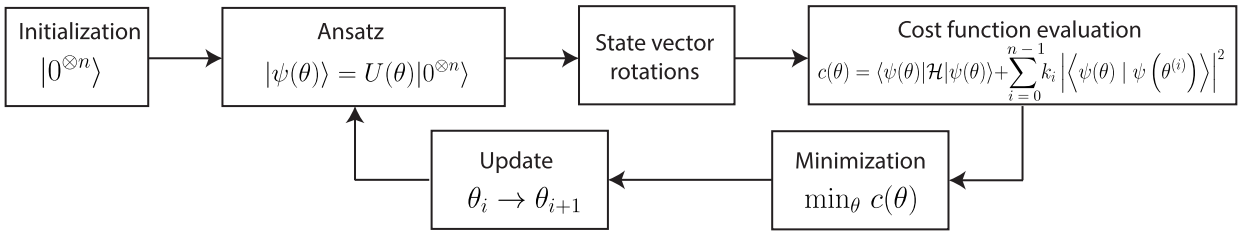

Fig. 3. Representative scheme of the VQE algorithm. Step 1, the n qubits are initialized to the state $|0\rangle$. Step 2, application of the parameterized unitary $U(\theta)$ to the initial state $|0^{\otimes n}\rangle$. Step 3, application of the quantum measurement circuits for the rotation of the quantum state vector for z-based measurements. Step 4, calculation of the cost function $c(\theta)$. Step 5, update of the θ_i parameters by the cost function minimization process.

TABLE I
NORMALIZED ENERGY LEVELS

Mode	Energy level	Computed value	Exact value
TM	E_0	$1.5313671 \cdot 10^5$	$1.5224093 \cdot 10^5$
	E_1	$6.0570108 \cdot 10^5$	$5.8578644 \cdot 10^5$
TE	E_0	$0.00175170 \cdot 10^5$	0
	E_1	$1.6633822 \cdot 10^5$	$1.5224093 \cdot 10^5$

The new points found are

$$x_{i+1} = x_i + \sum_{i=1}^{N} \alpha_i s_i \tag{21}$$

where $\sum_{i=1}^{N} \alpha_i s_i$ is the new search vector added to the search list. At each iteration, the vector that best satisfies the following condition:

$$\arg\max_{i=1}^{N} |\alpha_i| \|s_i\| \tag{22}$$

is removed from the search list. The algorithm stops when no improvement is made [34].

IV. RESULTS

The simulations for the TE and TM modes have been performed on a three-qubit quantum simulator, Qasm IBM Simulator. We consider the waveguide cross mapped onto a grid of 1 mm^2 cells for a total of 8 × 8 mm hollow metallic square waveguide. This choice is due to the possibility of obtaining solutions $|\psi\rangle$ of (8) of dimensions 2^3, due to quantum superposition for three qubit QC. The VQE algorithm was implemented using the Python-based quantum instruction kit (Qiskit) from IBM [35]. Qiskit is an open source IBM framework for working with QCs at the circuit, pulse and algorithm levels that allows us to simulate the results of a quantum circuit using different simulators. The framework also gives the possibility to transfer the code directly to real quantum hardware allowing for real measurements on multi-qubits hardware. Among the various simulators, the Qasm IBM Simulator was chosen, which is a shot-based simulator that runs quantum circuits by measuring the probability distribution of the different states, i.e., the bitstrings [28]. By default the Qasm IBM Simulator performs 1024 shots, therefore for more accurate results, 2^{13} shots have been chosen. This is the maximum number of shots that can be performed on this hardware. The energy values calculated following

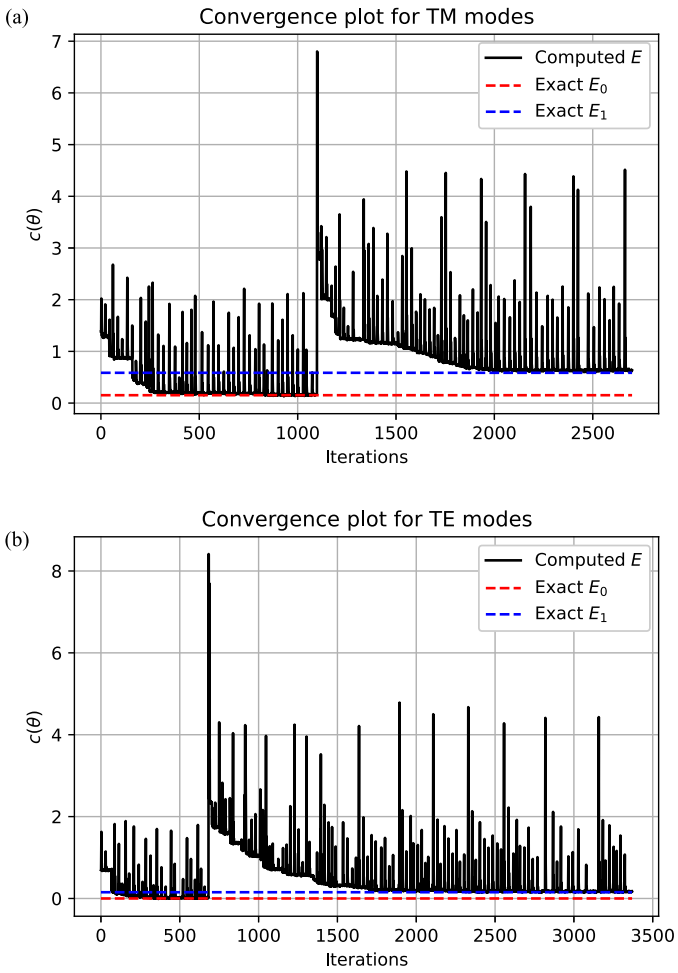

Fig. 4. (a) Convergence of the VQE algorithm for TM modes, (b) convergence of the VQE algorithm for TE modes. The calculated energy level E in (a) and (b) is shown in black, while the reference energy levels E_0 and E_1 related to the ground state and the first excited state are shown in red and blue, respectively.

optimization, the exact analytic values, the percentage error between the calculated and exact value, and the number of iterations are shown in Table I. After the simulation has run, the cost function plot converges toward the ground state energy E_0 and subsequently converges to the first excited state energy E_1 for both the TE and the TM modes are shown in Fig. 4. The values of E_0 and E_1 are known a priori, obtained by mathematically solving (1) and (2) for case reported in Fig. 2. Although the behavior of $c(\theta)$ is oscillatory, the minimum values of the oscillations converges to the analytical values previously obtained. The convergence is defined as an error

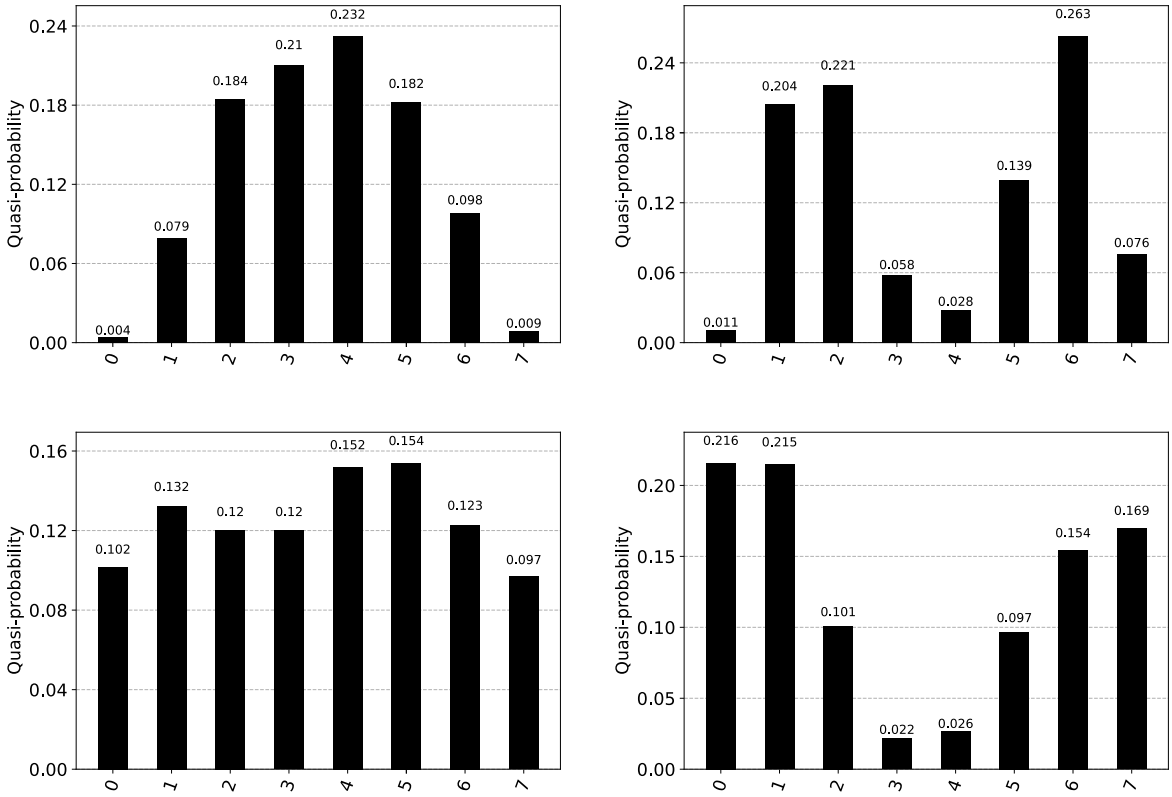

Fig. 5. Probability distribution of the ground state $|E_0\rangle$ and of the excited state $|E_1\rangle$ for the 1-D solutions of the TM and TE modes. The probability distribution of the state E_0 in the TM case is reported at the top left, the probability distribution of the state E_1 in the TM case is reported at the top right. The probability distribution of the state E_0 in the TE case is shown at the bottom left, the probability distribution of the state E_1 in the TE case is shown at the bottom right.

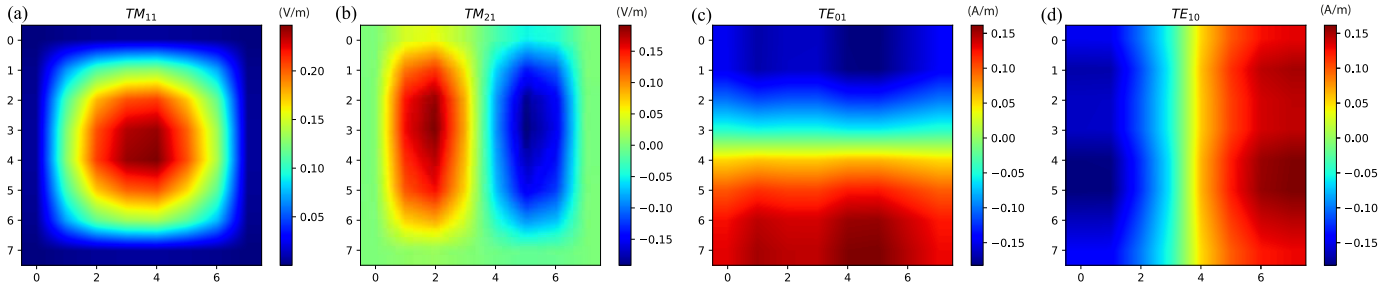

Fig. 6. Two-dimensional distributions of E_z and H_z inside a square waveguide. The grid consists of 8 × 8 cells of 1 mm^2. The TM and TE modes are obtained by the VQE algorithm on a three qubits quantum simulator. In (a) and (b) TM_{11} and TM_{21} mode are shown while in (c) and (d) TE_{01} and TE_{10} modes are reported. The values of the intensity of the fields are reported in the corresponding scales.

within 3% of the analytical value of the energies. In case of TM modes, the cost function converges to the ground state $|\psi_0\rangle$, also called $|E_0\rangle$, after 1124 iterations with the eigenvalue $E_0 = 0.15313671$, while it converges to the first excited state $|\psi_1\rangle$, also called $|E_1\rangle$, after 1613 iterations, with the eigenvalue $E_1 = 0.60570108$ as shown in Fig. 4 (top), for a total of 2727 iterations. In case of TE modes, the cost function converges to the ground state $|E_0\rangle$ after 629 iterations with the eigenvalue $E_0 = 0.00175170$, while it converges to the state $|E_1\rangle$ after 2746 iterations, with the eigenvalue $E_1 = 0.16633822$ as shown in Fig. 4 (bottom), for a total of 3375 iterations. The most precise value of the ground state (red line) has been found in the TM case with an absolute error of $e = 0.0008975$, while for the first excited state (blue line), the best result has been found for the TE case with an absolute error of $e = 0.01409729$. The probability distributions, as well as the square root of the absolute value of the solution of the Helmholtz equation for both the TE and the TM modes are shown in Fig. 5. On the horizontal axis the sequence $\{0, 1, 2, 3, 4, 5, 6, 7\}$ is encoded as the three qubit bitstrings $\{000, 001, 010, 011, 100, 101, 110, 111\}$, respectively. The probabilities are shown in the vertical axis. On the upper left corner, the probability distribution of the state $|E_0\rangle$ in the case of TM modes is reported. In particular, this state coincides with the square root of the absolute value of the Helmholtz solution for the ground state in the TM case. In the upper right corner, the probability distribution of the state $|E_1\rangle$, in the case of TE modes, is shown. In particular, this state coincides with the square root of the absolute value of the Helmholtz solution for the first excited state in TM case.

In the lower left corner, the probability distribution of the state $|E_0\rangle$ in the case of TE modes is reported. In particular, this state coincides with the square root of the absolute value of the Helmholtz solution for the ground state in the TE case. In the lower right corner, the probability distribution of the state $|E_1\rangle$ in the case of TE modes is reported. In particular, this state coincides with the square root of the absolute value of the Helmholtz solution for first excited state in the TE case. The electric field and magnetic field distributions for the modes TM_{11}, TM_{21}, TE_{10}, and TE_{01} are shown in Fig. 6. These 2-D distributions of the electric and magnetic fields are obtained starting from the states E_0 and E_1 for the TM and TE cases. In particular, the states represent the 1-D solution of the Helmholtz equation, i.e., with respect to x or y. To build the scalar maps, the two solutions are multiplied using a mesh grid defining the variation of the fields along the two axes. To obtain the mode TM_{11}, the product between $|E_0\rangle$ on x and $|E_0\rangle$ on y of TM solutions was carried out. For the mode TM_{21}, on the other hand, the product between $|E_1\rangle$ on x and $|E_0\rangle$ on y of TM solutions was carried out. In these cases, the variation of the electric field component E_z on the transversal section of the waveguide is represented. The way TE_{01}, the product between $|E_0\rangle$ on x and $|E_1\rangle$ on y of TE solutions was carried out. To obtain the mode TE_{10}, the product between $|E_1\rangle$ on x and $|E_0\rangle$ on y of TE solutions. In these cases, the variation of the magnetic field component H_z on the cross section of the waveguide is represented.

V. Conclusion

We have proposed a VQE algorithm for solving the waveguide modes on quantum simulator exploiting the quantum advantage of superposition and entanglement. In particular, shot-based simulations have been carried out to emulate the behavior of real quantum hardware accounting for the limitations of current implementations. First, the Helmholtz differential equation has been written into matrix form resulting in an eigenvalue equation associated with the Hamiltonian operator. Second, the Hamiltonian has been broken up into linear combination of Pauli strings consisting of Kronecker products of X, Y, Z, and I state vector rotation matrices. One of the current limitations of real QCs lies above z-axis of the Bloch sphere measurement without directly measuring the x and y components of the state vector. Thus, the basis change has been made by adding the measuring quantum circuits to the HEA for each simple observable of the Hamiltonian decomposition. Third, the cost function has been defined as a sum of the expectation value of the Hamiltonian $\langle H\rangle_\psi$ and the excitation term $\sum_{i=0}^{n-1} k_i|\langle\psi(\theta) \mid \psi(\theta^{(i)})\rangle|^2$. Hence, by minimizing the cost function $c(\theta)$ through the Powell optimization algorithm, the VQE algorithm has been able to find the ground state and the first excited state that correspond to the first two waveguide modes. The VQE algorithm proved to be a valid solution for solving electromagnetic problems allowing to use a small number of qubits to simulate larger domains with logarithmic complexity. In particular, the solution we proposed is based on simulating the probabilistic nature of real quantum hardware executable to current NISQ systems. The goal was to create a variational (universal gate) quantum circuit that completely emulates the probabilistic behavior of QCs to obtain the probability density distribution. The focus of the study was on defining the VQE to solve electromagnetic problems efficiently, i.e., overcoming hardware limitations such as the decomposition of the Hamiltonian in the Pauli basis and the related quantum measurement circuits. In future studies, the noise model for quantum gate and real measurements will be introduced to quantify the uncertainty of prediction. Introducing numerical noise models in the VQE shot-based simulations would lead to more accurate, efficient, and optimized quantum prediction algorithms for current and future NISQ systems. Moreover, thanks to the proof of principle provided by this work, it will be possible to simulate, more complex waveguide and cavity geometries [36], introduce non-homogeneous materials [37], [38], increase the number of qubits, and run the variational algorithm on real quantum hardware. The VQE represents an important solution for NISQ era that overcomes the limitations of limited number of qubits and limited quantum circuit depths, enabling academia and industry to find optimized codes to achieve quantum advantage.

Appendix
Quantum Measurement Circuits for the Quantum State Vector Rotation

The measurement circuits that allow the quantum state vector to rotate appropriately to carry out the measurements along z-axis for TM and TE modes are shown below.

The quantum measurement circuit for the observable IIX is represented as

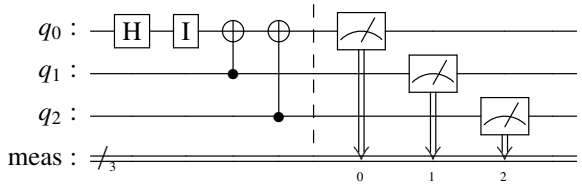

The quantum measurement circuit for the observable IXX is represented as

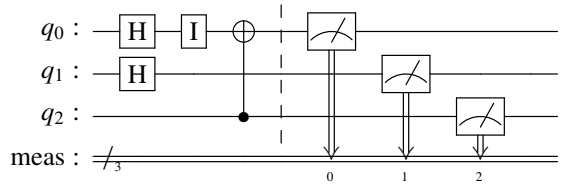

The quantum measurement circuit for the observable IYY is represented as

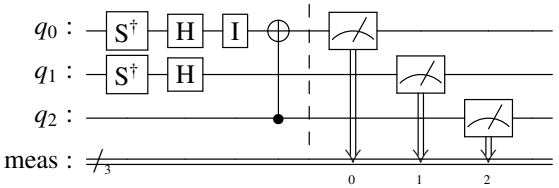

The quantum measurement circuit for the observable IZZ is represented as

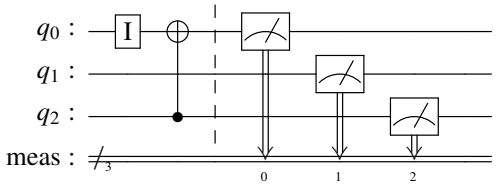

The quantum measurement circuit for the observable XXX is represented as

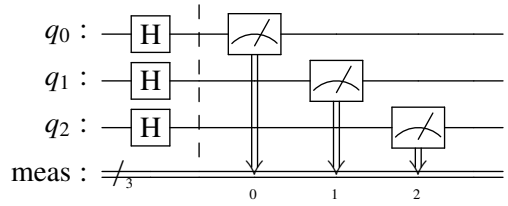

The quantum measurement circuit for the observable XYY is represented as

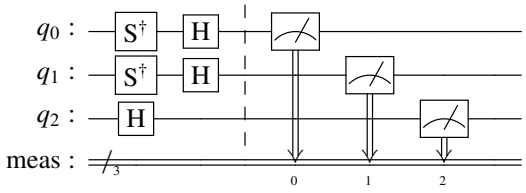

The quantum measurement circuit for the observable YXY is represented as

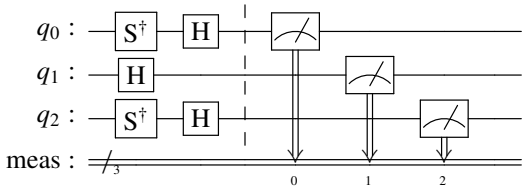

The quantum measurement circuit for the observable YYX is represented as

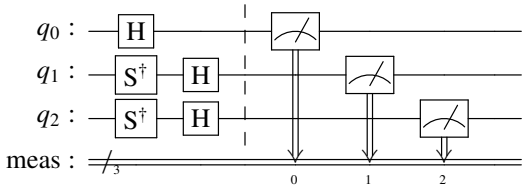

The quantum measurement circuit for the observable ZIZ is represented as

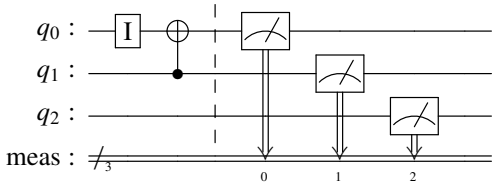

The quantum measurement circuit for the observable ZZI is represented as

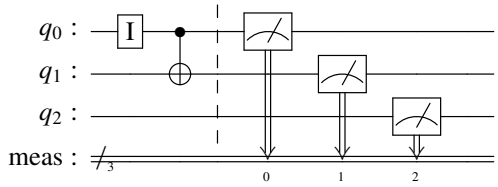

We have excluded the cases of the observables ZZZ and III.

REFERENCES

[1] M. Hirvensalo, *Quantum Computing*, 2nd ed. Heidelberg, Germany: Springer, 2004.

[2] J. L. Hevia, G. Peterssen, C. Ebert, and M. Piattini, "Quantum computing," *IEEE Softw.*, vol. 38, no. 5, pp. 7–15, Sep. 2021.

[3] R. P. Feynman, "Simulating physics with computers," *Int. J. Theor. Phys.*, vol. 21, nos. 6–7, pp. 467–488, Jun. 1982.

[4] D. P. DiVincenzo, "Quantum computation," *Science*, vol. 270, no. 5234, pp. 255–261, Oct. 1995.

[5] D. Aharonov, "Quantum computation," in *Annual Reviews of Computational Physics VI*. Singapore: World Scientific, 1999, pp. 259–346.

[6] A. J. Daley et al., "Practical quantum advantage in quantum simulation," *Nature*, vol. 607, no. 7920, pp. 667–676, Jul. 2022.

[7] E. Grumbling and M. Horowitz, *Quantum Computing: Progress and Prospects*. Washington, DC, USA: Nat. Academies Press, 2019. [Online]. Available: https://nap.nationalacademies.org/catalog/25196/quantum-computing-progress-and-prospects

[8] C. Neill et al., "A blueprint for demonstrating quantum supremacy with superconducting qubits," *Science*, vol. 360, no. 6385, pp. 195–199, Apr. 2018.

[9] G. Li, Y. Ding, and Y. Xie, "Tackling the qubit mapping problem for NISQ-era quantum devices," in *Proc. 24th Int. Conf. Architectural Support Program. Lang. Operating Syst.*, Apr. 2019, pp. 1001–1014.

[10] T. D. Ladd, F. Jelezko, R. Laflamme, Y. Nakamura, C. Monroe, and J. L. O'Brien, "Quantum computers," *Nature*, vol. 464, no. 7285, pp. 45–53, Mar. 2010.

[11] S. S. Tannu and M. K. Qureshi, "Not all qubits are created equal: A case for variability-aware policies for NISQ-era quantum computers," in *Proc. 24th Int. Conf. Architectural Support Program. Lang. Operating Syst.*, Apr. 2019, pp. 987–999.

[12] K. Bharti et al., "Noisy intermediate-scale quantum algorithms," *Rev. Mod. Phys.*, vol. 94, Feb. 2022, Art. no. 015004.

[13] M. Brooks. *What's Next for Quantum Computing*. Accessed: Jan. 6, 2023. [Online]. Available: https://www.technologyreview.com/2023/01/06/1066317/whats-next-for-quantum-computing/

[14] S. Endo, Z. Cai, S. C. Benjamin, and X. Yuan, "Hybrid quantum-classical algorithms and quantum error mitigation," *J. Phys. Soc. Jpn.*, vol. 90, no. 3, Mar. 2021, Art. no. 032001.

[15] W.-B. Ewe, D. E. Koh, S. T. Goh, H.-S. Chu, and C. E. Png, "Variational quantum-based simulation of waveguide modes," *IEEE Trans. Microw. Theory Techn.*, vol. 70, no. 5, pp. 2517–2525, May 2022.

[16] M. Cerezo et al., "Variational quantum algorithms," *Nature Rev. Phys.*, vol. 3, no. 9, pp. 625–644, 2021.

[17] S. S. Bharadwaj and K. R. Sreenivasan, "Quantum computation of fluid dynamics," 2020, *arXiv:2007.09147*.

[18] E. Colella et al., "Real-system variational quantum eigensolver for electromagnetic waveguides: A benchmark study," in *Proc. Int. Conf. Microw., Commun., Antennas, Biomed. Eng. Electron. Syst. (COMCAS)*, Tel Aviv, Israel, Nov. 2023, pp. 1–13.

[19] L. Tosi, P. Rocca, N. Anselmi, and A. Massa, "Array-antenna power-pattern analysis through quantum computing," *IEEE Trans. Antennas Propag.*, vol. 71, no. 4, pp. 3251–3259, Apr. 2023.

[20] C. Ross, G. Gradoni, Q. J. Lim, and Z. Peng, "Engineering reflective metasurfaces with Ising Hamiltonian and quantum annealing," *IEEE Trans. Antennas Propag.*, vol. 70, no. 4, pp. 2841–2854, Apr. 2022.

[21] N. Marcuvitz, *Waveguide Handbook* (IEE Electromagnetic Waves Series). New York, NY, USA: McGraw-Hill, 1951.

[22] T. K. Sarkar, K. Athar, E. Arvas, M. Manela, and R. Lade, "Computation of the propagation characteristics of TE and TM modes in arbitrarily shaped hollow waveguides utilizing the conjugate gradient method," *J. Electromagn. Waves Appl.*, vol. 3, no. 2, pp. 143–165, Jan. 1989.
[23] Q. J. Lim, C. Ross, A. Ghosh, F. Vook, G. Gradoni, and Z. Peng, "Quantum-assisted combinatorial optimization for reconfigurable intelligent surfaces in smart electromagnetic environments," *IEEE Trans. Antennas Propag.*, 2023.
[24] C. Li and F. Zeng, "Finite difference methods for fractional differential equations," *Int. J. Bifurcat. Chaos*, vol. 22, no. 4, p. 1230014, 2012.
[25] A. W. Harrow, A. Hassidim, and S. Lloyd, "Quantum algorithm for linear systems of equations," *Phys. Rev. Lett.*, vol. 103, no. 15, Oct. 2009, Art. no. 50502.
[26] D. Dervovic, M. Herbster, P. Mountney, S. Severini, N. Usher, and L. Wossnig, "Quantum linear systems algorithms: A primer," 2018, *arXiv:1802.08227*.
[27] Y. Sato, R. Kondo, S. Koide, H. Takamatsu, and N. Imoto, "Variational quantum algorithm based on the minimum potential energy for solving the Poisson equation," *Phys. Rev. A, Gen. Phys.*, vol. 104, no. 5, Nov. 2021, Art. no. 052409.
[28] M. A. Nielsen and I. L. Chuang, *Quantum Computation and Quantum Information*. Cambridge, U.K.: Cambridge Univ. Press, 2010.
[29] Y. Zhang, K. Lu, and Y. Gao, "QSobel: A novel quantum image edge extraction algorithm," *Sci. China Inf. Sci.*, vol. 58, no. 1, pp. 1–13, Jan. 2015.
[30] D. Maslov, "Advantages of using relative-phase Toffoli gates with an application to multiple control Toffoli optimization," *Phys. Rev. A, Gen. Phys.*, vol. 93, no. 2, Feb. 2016, Art. no. 022311.
[31] A. Peruzzo et al., "A variational eigenvalue solver on a photonic quantum processor," *Nature Commun.*, vol. 5, no. 1, Jul. 2014, Art. no. 4213.
[32] J. C. Butcher, *Numerical Methods for Ordinary Differential Equations*. New York, NY, USA: Wiley, 2016.
[33] S. Ramo, J. R. Whinnery, and T. Van Duzer, *Fields and Waves in Communication Electronics*, 3rd ed. New York, NY, USA: Wiley, 1994.
[34] R. Fletcher and M. J. Powell, "A rapidly convergent descent method for minimization," *Comput. J.*, vol. 6, no. 2, pp. 163–168, 1963.
[35] D. S. Steiger, T. Häner, and M. Troyer, "ProjectQ: An open source software framework for quantum computing," *Quantum*, vol. 2, p. 49, Jan. 2018.
[36] F. Moglie, L. Bastianelli, and V. M. Primiani, "Reliable finite-difference time-domain simulations of reverberation chambers by using equivalent volumetric losses," *IEEE Trans. Electromagn. Compat.*, vol. 58, no. 3, pp. 653–660, Jun. 2016.
[37] E. Colella, L. Bastianelli, V. M. Primiani, and F. Moglie, "Time reversal in reverberating environments for electromagnetic focusing in biological bodies," in *Proc. 3rd URSI Atlantic Asia–Pacific Radio Sci. Meeting*, Gran Canaria, Spain, May 2022, pp. 1–4.
[38] E. Colella, L. Bastianelli, F. Dragano, V. M. Primiani, and F. Moglie, "Time reversal in reverberating structures for deep focusing in human bodies," in *Proc. Int. Symp. Electromagn. Compat.*, Gothenburg, Sweden, Sep. 2022, pp. 141–144.

Emanuel Colella received the B.Sc. (Biomedical Engineer) and master's (cum laude) degrees in biomedical engineering from Università Politecnica delle Marche (UNIVPM), Ancona, Italy, in 2015 and 2019, respectively, where he is currently pursuing the Ph.D. degree in electromagnetics, with a focus on electromagnetic analysis of complex structures using classical and quantum algorithms.

In 2020, he was with the CNIT, as a Researcher for the RISE-6G project. He worked on computational electrodynamic simulations of RIS to analyze their performance in smart radio environment. Since 2022, he has been designated as the project lead of working group P2718 on the characterization of unintentional stochastic radiators. At 2023, he become a Principal Investigator for Non-standard Navy Cooperative Research and Development Agreement among the Naval Surface Warfare Center Dahlgren Division (NSWCDD), Dahlgren, VA, USA; the University of Surrey (UNIS), Guildford, U.K.; and UNIVPM for quantum computational electromagnetics (QCEM).

Spencer Beloin received the bachelor's degree in physics from the University of Georgia, Athens, GA, USA, in 2013, where he completed research in resolving fast optical signals. He is currently pursuing the Ph.D. degree at the Physics and Astronomy Department, University of Tennessee, Knoxville, TN, USA.

He is a Physicist with the United States Department of the Navy, Monterey, CA, USA. He subsequently joined the Physics and Astronomy Department, University of Tennessee, as a Research Assistant of theoretical nuclear physics. Since arriving at Dahlgren, he has researched weak-value amplification and the capability of quantum machines to solve various problems in physics.

Luca Bastianelli (Member, IEEE) received the M.S. and Ph.D. degrees in electronic engineering from Università Politecnica delle Marche, Ancona, Italy, in 2014 and 2018, respectively. During the Ph.D. degree, he spent seven months with the University of Nottingham, Nottingham, U.K.

In 2018, he was a Research Fellow with the Dipartimento di Ingegneria dell'Informazione, Università Politecnica delle Marche, where he is currently a Researcher with the CNIT. He is involved in the area of electromagnetic compatibility, telecommunications, and computational electrodynamics. He was involved in many PRACE projects. He currently leads the FDTDLIME project on reconfigurable intelligent surfaces and the H2020 RISE-6G project. His research interests include reverberation chambers, wave chaos, propagation in complex systems, ray tracing, time reversal, metasurfaces, 5G, and numerical techniques on high performance computers.

Dr. Bastianelli was a member of the COST Action IC1407 ACCREDIT. He is currently an active member of the working group for the development of the IEEE Standards P2718 on near field characterization. He received the URSI Commission E Young Scientist Award in 2017. During his fellowship, he is involved in teaching support activities.

Valter Mariani Primiani (Senior Member, IEEE) received the Laurea degree (summa cum laude) in electronic engineering from the University of Ancona, Ancona, Italy, in 1990.

He is currently a Professor of electromagnetic compatibility (EMC) with Università Politecnica delle Marche, Ancona. He is a member with the Department of Information Engineering, where he is also responsible for the EMC Laboratory. Since 2003, he has been involved in research activities on the application of reverberation chambers for compliance testing and for metrology applications. He is a member with the COST Action 1407 ACCREDIT on the characterization of stochastic emissions from digital equipment. Since 2021, he has been involved in the RISE–6G project. His research interests include the prediction of digital printed circuit board radiation, the radiation from apertures, the electrostatic discharge coupling effects modeling, and the analysis of emission and immunity test methods.

Prof. Mariani Primiani is a Senior Member of the IEEE (EMC society) and a member of the Italian Society of Electromagnetics. From 2007 to 2013, he was an active member of the working group for the development of the IEEE Standards: 299.1-2013 on shielding effectiveness measurements. Since 2014, he has been a member of the International Steering Committee of EMC Europe. He is in the World's Top 2% Scientists by Elsevier, in October 2022 and November 2023. He is currently an Associate Editor of the *IET Science, Measurement and Technology* journal.

Franco Moglie (Senior Member, IEEE) received the "Dottore Ingegnere" degree in electronics engineering from the University of Ancona, Ancona, Italy, in 1986, and the Ph.D. degree in electronics engineering and electromagnetics from the University of Bari, Bari, Italy, in 1992.

Since 1986, he has been a Research Scientist with Università Politecnica delle Marche, Ancona, where he has been an Associate Professor, since 2016. In 2007, he is or was an active member with some working groups for the development of IEEE Standards: 299.1, 1302, 2715, and 2716. Since 2007, he has been a member with the "Accademia Marchigiana di Scienze, Lettere ed Arti–Istituto Culturale Europeo" (Marches Academy of Sciences, Arts and Letters–European Cultural Institute), which is based in Ancona. Since 2011, he has been with the Department of Information Engineering. In 2011, he was a Visiting Researcher with the Wave Chaos Group, IREAP, University of Maryland, College Park, MD, USA. From 2013 to 2019, he led three PRACE high performance computing projects on reverberation chambers. Since 2014, he has been an Italian Management Committing Member of the COST Action IC1407. Since 2017, he has been the Secretary of the working group for the IEEE Standard 2718. Since 2021, he has been the Scientific Manager with the CNIT, Università Politecnica delle Marche in the RISE–6G project. His current research interests include EM numerical techniques. In particular, his research activity is in the field of the application of reverberation chambers for compliance testing, metrology applications, and multipath propagation.

Dr. Moglie is a member of the IEEE Electromagnetic Compatibility Society and the Italian Electromagnetics Society. In 2013, he received the title of Distinguished Reviewer of IEEE TRANSACTIONS ON ELECTROMAGNETIC COMPATIBILITY. He is in the World's Top 2% Scientists by Elsevier, in October 2022 and November 2023.

Gabriele Gradoni (Member, IEEE) received the Ph.D. degree in electromagnetics from Università Politecnica delle Marche, Ancona, Italy, in 2010.

He was a Visiting Researcher with the Time, Quantum, and Electromagnetics Team, National Physical Laboratory, Teddington, U.K., in 2008. From 2010 to 2013, he was a Research Associate with the Institute for Research in Electronics and Applied Physics, University of Maryland, College Park, MD, USA. From 2013 to 2016, he was a Research Fellow with the School of Mathematical Sciences, University of Nottingham, Nottingham, U.K., where he has been a Full Professor of mathematics and electrical engineering, since 2023. Since 2020, he has been a Royal Society Industry Fellow at British Telecommunications, U.K., and has been an Adjunct Associate Professor with the Department of Electrical and Computer Engineering, University of Illinois at Urbana Champaign, Champaign, IL, USA. Since December 2022, he has been a Visiting Fellow with the Department of Computer Science and Technology, University of Cambridge, U.K. His research interests include probabilistic and asymptotic methods for propagation in complex wave systems, wave chaos, and metasurfaces, with applications to electromagnetic compatibility and modern wireless communication systems.

Dr. Gradoni is a member of the American Physical Society and the Italian Electromagnetics Society. He received the URSI Commission B Young Scientist Award in 2010 and 2016, the Gaetano Latmiral Prize in 2015, the Honorable Mention IEEE TEMC Richard B. Schulz Transactions Prize Paper Award in 2020, and the EuCAP Best Electromagnetics Paper Award in 2021. From 2014 to 2021, he has been the URSI Commission E Early Career Representative.

Open Access funding provided by 'Università Politecnica delle Marche' within the CRUI CARE Agreement